SB^{3}C2017
Summer Biomechanics, Bioengineering and Biotransport Conference
June 21 – 24, Tucson, AZ, USA

FINITE ELEMENT METHOD FOR PREDICTING FAILURE LOCATION OF ANNULUS FIBROSUS IN UNIAXIAL TENSION

Benjamin Werbner*, Minhao Zhou*, Grace O'Connell

Mechanical Engineering
University of California, Berkeley
Berkeley, CA, United States

INTRODUCTION

Fiber-reinforced tissues experience large, complex loads during daily activities. Failure of these tissues often results in debilitating pain and reduced mobility. Understanding the failure behavior of tissues with limited self-healing capabilities, such as annulus fibrosus (AF) in the intervertebral disc, is of particular importance, as their failure may transfer stresses to adjacent tissues, resulting in a cascade of damage and degeneration [1].

Unfortunately, the failure mechanics of fiber-reinforced tissues, particularly those with fibers oriented off-axis from the applied load, is not well understood. Previous studies have suggested that this is due to limited specimen sizes and high strains at the testing grips, which may cause unpredictable tissue failure [2, 3]. Recent work by Peloquin *et al.* identified five different failure modes in meniscus specimens, with less than 25% of specimens failing at the mid-substance [3]. Such unpredictable failure behavior may be responsible for the large variation of failure properties reported in the literature.

Finite element models (FEMs) are powerful tools that can provide insight into local tissue deformations that are difficult or impossible to measure experimentally [4]. Moreover, FEMs are valuable tools for directing and guiding time-intensive experimental studies. By utilizing both finite element models and mechanical testing, we aimed to develop and validate a robust testing protocol to investigate failure properties of annulus fibrosus. In particular, the geometries of experimental test specimens were designed based on simulation results. This study focused on AF tissue, a complex angle-ply laminate structure composed of alternating layers of fibers oriented between ±30° and ±45° to the transverse plane [5]. The findings presented here, however, are applicable to other fiber-reinforced materials as well.

METHODS

Modeling: FEMs were developed representing rectangular AF specimens oriented in the circumferential-axial direction (circ.-ax., Fig 1A) (PreView 1.19.0; FEBio 2.5.2; ~180k nodes, ~170k hexahedral elements). Bulk tissue dimensions were defined to be 4.8 mm x 2 mm x 0.8 mm, which is proportional to experimental samples from our previous work [5]. Four 200 μm-thick, welded-interface lamellae were included with fibers oriented at ±30° to the transverse plane to represent outer AF, and with fibers oriented at ±45° to represent inner AF [6]. Full-width sandpaper grips were simulated to cover 0.4 mm of the tissue at both ends. A homogeneous, hyperelastic material description was used [7], with material coefficients based on preliminary tests of circ.-ax. AF in tension (ρ= 1 g/cm^3, C_1= C_2 = 0.1 MPa, C_3= 0.02 MPa, C_4= 30, C_5= 25 MPa, k= 50 MPa, λ= 1.15).

In addition to the 'Intact' model, two notch geometries were evaluated. For the first notch geometry, a 2 mm x 0.04 mm x 0.04 mm block of material was removed at the mid-substance (MS), such that half of the original cross-sectional area remained (Fig. 1B- 'Half'). The second notch geometry was created by removing material from the remaining region, such that one quarter of the original cross-sectional area remained (Fig. 1B- 'Quarter').

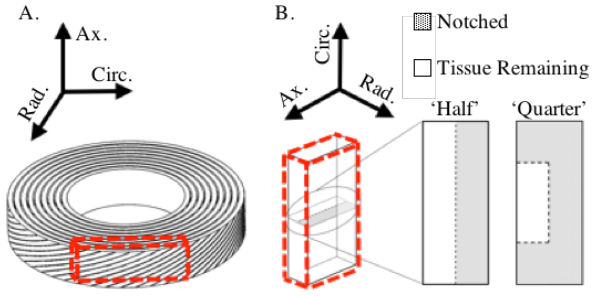

Fig. 1: A. Specimen orientation and B. notch geometries

Simulated loading was applied in two stages: a 10% compressive strain was applied at the gripped region, followed by uniaxial tension to 30% global engineering strain along the specimen length. Boundary conditions at the grips were fixed to represent no slipping between the grips and the sample surface.

Local strains for each node in the mid-substance and at the grip-line were sorted in descending order, and the average strain for each region was calculated as the average of the top 35 nodes. Then, the MS:grip strain ratio was calculated as the average mid-substance local strain divided by the average grip-line local strain. An MS:grip strain ratio greater than 1.0 indicates that the average strain is higher at the mid-substance than at the grip. Average local strain of 65% served as an estimate of bulk failure initiation, and failure was predicted at the location reaching this strain threshold earliest in the simulation.

Experimental: Healthy intervertebral discs were dissected from mature bovine caudal spines. Rectangular tissue sections oriented in the circ.-ax. direction were isolated from the outer-middle annulus, and parallel surfaces were created using a freezing stage microtome (thickness = 2 mm; Intact, n = 6). For Half notch specimens, a full-width (5.2 ± 0.6 mm) notch was created using a scalpel and depth-stop, resulting in a final thickness of 1 mm at the mid-substance (n = 8). For Quarter notch samples, additional cuts were made to further reduce the cross-sectional area to a final width of 2.9 ± 0.3 mm (n = 8).

Each sample was superglued into sandpaper, which was secured into a custom saline water bath attached to an Instron testing machine. A 0.05 N pre-load was used to remove slack before imaging the specimens with a scale bar to determine the exact width and length before testing. Uniaxial tension was applied at a rate of 50 mm/min. Lagrangian strain was calculated as the change in displacement divided by the initial grip-to-grip distance. Stress was calculated by dividing the measured force by the mid-substance cross-sectional area. Failure stress was defined as the maximum stress recorded during the test, and failure strain was defined as the strain corresponding with the failure stress. Toe- and linear-region moduli were calculated using a custom bi-linear fit to the stress-strain response.

RESULTS

Modeling: The model fit well to the nonlinear, experimental stress-strain data (R = 0.99). Average local strains reached 65% at either the mid-substance or at the grip-line for all simulations. For Intact and Half notch simulations, the average local strain was always higher at the grip-line than at the mid-substance by at least 15% (Fig. 2- black arrows; Fig. 3- red and green lines), so the model predicts grip-line failure in these samples. In Quarter notch simulations, maximum local strain at failure occurred at the notch site (Fig. 2- white arrows; Fig. 3- black and blue lines), so the model predicts mid-substance failure in these samples.

For inner-middle AF tissue, which has fibers oriented at ±45° from the loading direction, failure was strongly predicted to occur at the mid-substance (Fig. 3- black line, MS:grip ratio = 2.52). Outer AF, which has fibers oriented at ±30° from loading, was also predicted to fail at the mid-substance, but with less certainty, due to the low MS:grip ratio (1.04) at the time of predicted failure (Fig. 3- blue line).

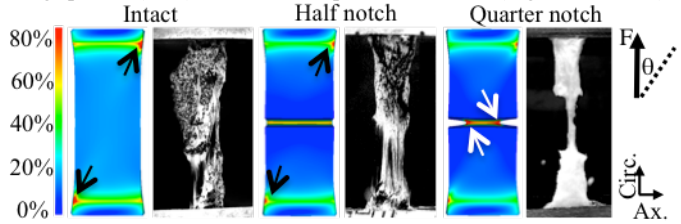

Fig. 2: Strain map at predicted failure initiation (arrows at max. local strain) and images of mechanical test specimens at failure.

Experimental: All samples tested exhibited a nonlinear stress-strain response. Bulk tissue failure originated at the grip-line in 100% of Intact samples and in 75% of Half notch samples. Quarter notch samples failed robustly within 2 mm of the mid-substance for all but one specimen (88%). Failure stress, failure strain, and toe- and linear-region moduli for the Quarter notch samples that failed at the mid-substance were 4.93 ± 1.07 MPa, 52% ± 7%, 1.55 ± 0.17 MPa, and 19.25 ± 3.27 MPa, respectively.

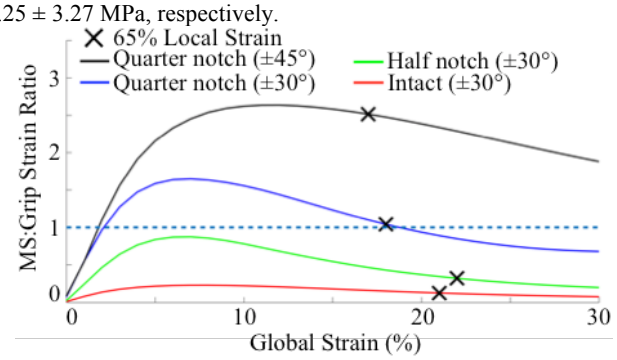

Fig. 3: MS:grip strain ratio vs. global strain for three notch geometries, including two fiber angles. X denotes predicted failure.

DISCUSSION

We investigated the effectiveness of using an FEM to predict the failure location of annulus fibrosus tissue samples with different mid-substance notch geometries. Repeatable mid-substance failure was achieved only in Quarter notch samples, which represent a modified dog-bone geometry. FEM results were validated with experimental tests. The standard deviations for material properties of Quarter notch specimens were less than 22% of the mean, which is low compared to data in the literature (>25%) [8-10]. The simulations indicate that grip-line failure was the result of higher compressive strains from gripping outweighing tensile strains at the mid-substance. Therefore, it is essential to model grip effects when investigating failure properties.

Our previous work used a Half notch geometry to induce repeatable mid-substance failure in circumferential-radial AF samples [5], suggesting that specimens with shorter fiber bundles tend to have higher MS:grip strain ratios. Additionally, the results of this study indicate that specimens with fibers more aligned with the loading direction are more likely to fail at the grip-line, thus mid-substance failure is more likely in inner- and middle-AF specimens.

We used a pre-defined strain threshold of 65% to predict tissue failure due to the lack of experimental data providing local failure strains. Furthermore, our model did not include a description for damage, resulting in a significant difference between the models' predicted bulk failure around 20% global strain and experimentally measured bulk failure at ~50% global strain. Future work will utilize a heterogeneous model that incorporates the tissue's micro-mechanical structure. This model will allow us to include corresponding damage descriptions to better investigate mechanisms of AF tissue failure [7].

This study used a combined approach of computational modeling and mechanical testing to develop and validate a method for sample preparation. Our approach focused on ensuring mid-substance failure of AF, which is a complex fiber-reinforced tissue with fibers aligned off-axis from the applied load. In conclusion, the combined method facilitates efficient and accurate evaluation of AF failure location.

ACKNOWLEDGEMENTS *Both authors contributed equally.

REFERENCES [1] Adams, M.+, *Spine*, 2006; [2] Jacobs, N.+, *J Biomech Eng*, 2013; [3] Peloquin, J.+, *J Biomech Eng*, 2016; [4] Schmidt, H.+, *J Biomech*, 2013; [5] Werbner, B.+, *ORS*, 2017; [6] Cassidy, J.+, *Conn Tiss*, 1989; [7] Yang, B.+, *SB3C*, 2016; [8] Green, T.+, *Eur Spine J*, 1993; [9] Acaroglu, E.+, *Spine,* 1995; [10] O'Connell, G.+, *J Biomech Eng*, 2009.